Chapter 3

Carbon flow through a benthic food web: Integrating biomass, isotope and tracer data

Dick van Oevelen, Karline Soetaert, Jack J. Middelburg, P. M. J. Herman, Leon Moodley, Ilse Hamels, Tom Moens and Carlo H. R. Heip. *Submitted to Journal of Marine Research*

3.1 Introduction

The food web is a central concept in ecology and the herbivorous, detrital and microbial pathways are among its major carbon transfers. Much ecological theory is centered around the herbivorous food chain, in which primary producers sustain higher trophic levels (Ryther, 1969; Steele, 1974; Oksanen et al., 1981). The importance of the detrital pathway has been emphasized by Teal (1962) and Odum (1969) and is supported by empirical evidence (Polis and Hurd, 1996; Pace et al., 2004). More recently, the microbial loop was formalized as the transfer of dissolved organic matter, originating from phytoplankton exudation or sloppy feeding (Jumars et al., 1989), through bacterial assimilation and several grazing transfers to larger zooplankton (Azam et al., 1983). In natural food webs these three pathways are linked in many ways (Polis and Strong, 1996) and elucidating these linkages poses a major challenge in community ecology (Legendre and Rassoulzadegan, 1995; Polis and Strong, 1996; Herman et al., 1999; Cebrian, 2004; Moore et al., 2004).

Temperate intertidal flat communities are heterotrophic systems (Heip et al., 1995) and receive carbon inputs from local primary production by microphytobenthos, deposition of high-quality phytodetritus and low-quality organic matter associated with suspended particles from the water column and active filtration by suspension feeders (Herman et al., 1999). The high metabolic activity driven by this wide spectrum of organic matter sources renders intertidal flats excellent arenas to study the importance of the different pathways in natural food webs.

However, quantifying natural food webs is a notorious problem, as methodological and logistical limitations impede simultaneous measurement of all flows. Klepper and Van de Kamer (1987) and Vézina and Platt (1988) pioneered inverse analysis, a data assimilation technique that merges field observations and a priori literature information in a food web

structure, to quantify the unmeasured flows. Inverse analysis has been developed in the geophysical sciences (Wunsch and Minster, 1982; Menke, 1984) and has proven to be a robust means to capture the main food web characteristics (Vézina and Pahlow, 2003; Vézina et al., 2004).

In this paper we first extend the inverse methodology, to resolve not only conventional standing stock and process measurements, but also natural abundance stable isotope signatures and transient tracer data. This extended methodology was applied to a large data set on the food web of the Molenplaat intertidal flat (The Netherlands) (Herman et al., 2001). The data set contained different types of data: biomass of the benthos, carbon production and processing (Herman et al., 2001), integrated diet information from stable isotope signatures (Herman et al., 2000; Moens et al., 2002) and tracer data on the fate of recently fixed carbon by local primary producers (Middelburg et al., 2000). The use of all these data resulted in a significantly better constrained food web, as shown by uncertainty analysis. The resulting food web characteristics are discussed with respect to the importance of and linkages among the herbivorous, detrital and microbial pathways.

3.2 Methods

3.2.1 Study area, food web structure and data

The Molenplaat intertidal flat is located in the saline part (salinity 20-25) of the turbid, nutrient-rich and heterotrophic Scheldt estuary (Belgium, The Netherlands). The study site (station MP2 in the ECOFLAT-project) has a silt content of 38 % and organic carbon content of 0.70 % wt/wt. Herman et al. (2001) provide detailed information on the study site.

The specification of food web compartments is based on the conventional distinction based on size classes (e.g. Schwinghamer (1981)) and we consider microphytobenthos, bacteria, microbenthos (i.e. flagellates and ciliates), nematodes and other meiobenthos (copepods, ostracods and foraminifera) and macrobenthos (deposit and suspension feeders) (Fig. 3.1). Nematodes are treated separately from the other meiobenthos, because data on feeding preferences and tracer incorporation were available only for nematodes. Additionally, two abiotic carbon compartments are defined: particulate detritus and dissolved organic carbon (DOC), the latter including extracellular polymeric substances (EPS).

Extensive sampling was conducted between 1996 and 1999. Carbon stocks of detritus and all biotic compartments were determined from sediment cores. Total carbon processing was measured with field and laboratory incubations, yielding data on benthic primary production, bacterial secondary production, bacterivory by microbenthos and community respiration (Table 3.1). Nematode mouth morphology was investigated to determine the feeding preferences of the nematode community (Steyaert et al., 2003).

Natural abundance δ^{13}C isotope signatures provide an integrated measure of the different diet contributions to an organism. The δ^{13}C of nematodes, meiobenthos and macrobenthos was determined from hand-picked specimens and the bacterial δ^{13}C was derived from the δ^{13}C of bacterial specific polar lipid derived fatty acids (PLFAs) (Table 3.1). The δ^{13}C of detritus was calculated from depth profiles of δ^{13}C of total particulate organic matter (Table 3.1).

The fate of microphytobenthic carbon was quantified by an in situ pulse-chase experiment (Middelburg et al., 2000). Intertidal microphytobenthos only fixes carbon during the sunlit period of emersion, because the high turbidity of the Scheldt

estuary prevents light from reaching the sediment during submersion. During emersion, ^{13}C-HCO_3^- was sprayed on the surface of the tidal flat and was fixed by microphytobenthos. Subsequently, the ^{13}C tracer was tracked in bacteria, nematodes and macrobenthos, providing quantitative data on the transfer of recently fixed microphytobenthic carbon through the food web.

In addition to site-specific data, an extensive literature review was conducted to obtain quantitative information on processes for which direct field observations were not available and these data were used to constrain unknown flows within biological realistic bounds. Constraints were placed on 1) respiration and EPS excretion by microphytobenthos, 2) bacterial growth efficiency, 3) production rates, growth efficiency and assimilation efficiency of microbenthos, nematodes, meiobenthos and macrobenthos and 4) feeding preferences of nematodes and macrobenthos. Appendix A provides a complete listing, including references.

Table 3.1: Field observations used in the inverse analysis. Depth is the depth of integration. Sources are 1) Middelburg et al. (2000), 2) Hamels et al. (1998), 3) Hamels et al. (2004), 4) Steyaert et al. (2003), 5) L Moodley (unpub data), 6) Herman et al. (2000), 7) Hamels et al. (1998), 8) Dauwe et al. (2001), 9) Moens et al. (2002) and 10) PMJ Herman (unpub data).

Stocks mg C m^{-2}	**Depth (cm)**	**Value**	**Source**
Microphytobenthos[a]	8.5	2090	1
Bacteria	4.0	4097	2
Microbenthos	4.0	140	2,3
Nematodes	6.0	156	4
Microvores		4.0	
Ciliate feeders		59.2	
Deposit feeders		27.6	
Epistrate feeders		25.6	
Facultative predators		32.8	
Predators		7.2	
meiobenthos	1.0	259	5
Copepods		59.8	
Ostracods		38.5	
Foraminifera		161.1	
macrobenthos	20.0	12172	6
Suspension feeders		3639	
Deposit feeders		6270	
Surface deposit feeders		2264	
detritus	5.0	130660	6
doc[b]	5.0	336	
Rates mg C m^{-2} d^{-1}	**Depth (cm)**	**Value**	**Source**
Gross primary production	-	714	7
Community respiration	-	2112	8
Bacterial production[c]	0.3	598	2
Bacterial production	4.0	4121	2
Bacterivory microbenthos	4.0	13	2
δ^{13}C values	**Depth (cm)**	**Value**	**Source**
Microphytobenthos	-	-15.0	6
Bacterial PLFA	3.0	-20.4	1
Nematodes	4.0	-17.4	9

Meiobenthos	1.0	-15.3	5
Macrobenthos	20.0	-17.8	6
Detritus	30.0	-21.2	10
Phytoplankton	-	-21.0	6
Suspended particulate matter	-	-24.0	6

[a] Taken from the depth integrated chlorophyll *a* and assuming a carbon to chlorophyll *a* ratio of 40
[b] Assuming a DOC concentration of 800 μmol C l^{-1} for porewater and a porosity of 0.70
[c] Bacterial production used in the model is integrated to 0.3 cm (see 3.3 Results and 3.4 Discussion)

3.2.2 Inverse model formulation and uncertainty analysis

The goal of an inverse model is to quantify all flows that are present in a food web. The starting points is a topological food web. A topological web is a food web with flows being either present or absent and defines the mass balance for each food web compartment. Subsequently, quantitative information is added to the inverse model. For example, an equation can be added such that the sum of respiration flows equals the measured community respiration. Additionally, data from the literature are used to put biologically realistic bounds on the unmeasured flows, e.g. the assimilation efficiency can be constrained between a lower and upper boundary.

In this paper we develop the inverse model in three successive steps. First, the conventional methodology is applied, in which data on biomass and total carbon processing are used together with literature data to quantify the food web. Secondly, δ^{13}C stable isotope data are appended to the inverse model. Thirdly, data from an isotope tracer experiment are assimilated in the food web reconstruction. The inverse solutions will be referred to as: CS (Conventional Solution), CIS (Conventional and stable Isotope Solution) and CITS (Conventional, stable Isotope and Tracer Solution). The inverse models are implemented in the modeling environment FEMME (Soetaert et al., 2002) and can be freely downloaded from http://www.nioo.knaw.nl/ceme/femme.

Conventional inverse analysis (CS)

An inverse analysis model is expressed as 1) a set of linear equality equations

$$\mathbf{A}_{m,n}\mathbf{x}_n = \mathbf{b}_m \tag{3.1}$$

and 2) a set of linear constraint equations

$$\mathbf{G}_{m_c,n}\mathbf{x}_n \geq \mathbf{h}_{m_c} \tag{3.2}$$

Each element in $\mathbf{x}$ represents a food web flow and inverse analysis quantifies all n flows in $\mathbf{x}$. The equality equation (Eqs. 3.1) contains both the topological food web (i.e. the mass balances) and the field observations consisting of process data (Vézina and Platt (1988)). Each mass balance or observation fills one row in $\mathbf{A}$ and $\mathbf{b}$, m is therefore total number of mass balances and observations. A mass balance is expressed on row i of $\mathbf{A}$ as a combination of the food web flows in $\mathbf{x}$: the element $a_{i,j}$ is -1 when flow j is an outflow, 0 when flow j is not part of the mass balance or 1 when flow j is an inflow. The

increase or decrease of a compartment with time (i.e. $\frac{dC}{dt}$) enters b_i. Here we assume steady-state, which means that the sum of inflows equals the sum of outflows and $\frac{dC}{dt}$ is zero. Process data are added similarly as the mass balances: the elements in $\mathbf{A}$ express the contribution of the different flows to the process, e.g. community respiration is the sum of all respiration flows and the numerical data enter $\mathbf{b}$. The constraint equation is used to place upper or lower bounds on single flows or combinations of flows and these bounds will be respected in the inverse solution. The absolute values of the bounds are in vector $\mathbf{h}$ and the constraints coefficients, signifying whether and how much a flow contributes to the constraint, are in matrix $\mathbf{G}$.

Inverse food web models have typically less equality equations than unknown flows (i.e. $m < n$, Vézina and Platt (1988)), this means that an infinite number of solutions obey the equality and constraint equations. The conventional procedure is to select the solution (CS) that is minimal in the sum of squared flows (i.e. $\sum_{i=1}^{n} x_i^2$). This solution is regarded as the simplest or most parsimonious food web (Vézina and Platt, 1988). Appendix A contains all inverse model equations and constraints.

Introducing stable isotope data (CIS)

Natural abundance stable isotope data are typically interpreted by means of a linear mixing model to estimate diet contributions of a consumer (Phillips, 2001; Post, 2002). The δ^{13}C signature of a consumer ($\delta^{13}C_j$) is expressed as a weighted average of the isotope signatures of its resources ($\delta^{13}C_i$), fractionation (Δ_i) and the associated flow ($f_{i\to j}$)

$$\delta^{13}C_j = \frac{\sum_i (\delta^{13}C_i + \Delta_i) f_{i\to j}}{\sum_i f_{i\to j}} \tag{3.3}$$

Fractionation of ^{13}C with trophic level is very small $\sim$ 0.4 ‰ (Post, 2002) and is therefore neglected in our analysis. When all stable isotope signatures are known, they are easily implemented in the equality equation (Eqs. 3.1), but when isotope data for some compartments are missing a more complicated procedure is required (details in Appendix B). Briefly, an upper and lower boundary for each missing signature is assigned and the resulting parameter space is scanned with a grid search to locate the most parsimonious solution. Hence, the CIS is the parsimonious solution that satisfies the conventional and stable isotope data.

Assimilating deliberate tracer data (CITS)

Jackson and Eldridge (1992) simulated the fate of a tracer introduced in a pelagic food web inferred by inverse analysis. This approach inspired us to further increase the amount of data used in the food web reconstruction by adding data from a pulse-chase labeling of microphytobenthic carbon (see Appendix B for a detailed methodological description). Briefly, we generated a large set of inverse food webs and each food web was different in its flow values, but all satisfied the conventional and stable isotope data. Subsequently, each food web was fed to a tracer model that simulates tracer dynamics in each compartment. The modeled tracer dynamics were evaluated against the experimental data and the food web solution that optimally reproduced the tracer data was accepted as CITS.

Whereas in the tracer model of Jackson and Eldridge (1992) all incoming tracer instantly and homogeneously mixes in the receiving compartment, it is commonly found that metabolic processes are paid from a small pool with a comparatively fast turnover, e.g. respiration (Kooijman, 2000). Similarly, it is recently fixed carbon that is excreted as

extracellular polymeric substances (EPS) by microphytobenthos (Wolfstein et al., 2002). Therefore we assumed that respiration, excretion and faeces production have a tracer concentration equal to that of the incoming flows. Other outgoing flows, i.e. grazing, predation or export have the tracer concentration of the biotic compartment. Appendix B contains all model equations.

Uncertainty analysis

In accordance with the three step inverse analysis approach, we calculated the uncertainty for each food web. The uncertainty is expressed as flow ranges of the conventional solution (CSrange), ranges of conventional and stable isotope solution (CISrange) and ranges of conventional, stable isotope and tracer solution (CITSrange). The uncertainty analysis of CSrange and CISrange is based on subsequently minimizing and maximizing each flow (see Klepper and Van de Kamer (1987) and Stone et al. (1993))

$$\text{minimize } x_i \quad \text{and} \quad \text{maximize } x_i$$

under the conditions

$$\mathbf{Ax} = \mathbf{b}, \quad \mathbf{Gx} \geq \mathbf{h}$$

This analysis produces an envelope around each flow, which is interpreted as the potential range that a flow can attain given the data specified in the equality (either without (CSrange) or with (CISrange) the stable isotope signatures) and constraint equation. From all food webs that were ran in the tracer model, the best 10 % were used to determine CITSrange. The CITSrange was defined as the minimum and maximum of each flow found within the set of best solutions.

The effect of the uncertainty of the food webs on the tracer dynamics is presented in two ways: 1) as the lower and upper extremes in tracer dynamics found for each compartment when evaluating the large set of generated inverse solutions, therefore this represents the uncertainty in the tracer simulation of CIS and 2) after assimilating the tracer data as the lower and upper extremes in tracer dynamics for each compartment from the set of 10 % best food webs (CITSrange).

3.3 Results

3.3.1 Inverse solutions and uncertainty analysis

An initial attempt to solve the inverse model failed as a result of inconsistencies between field and literature data. Reconciliation of the depth-integrated bacterial production and community respiration required a bacterial growth efficiency of > 0.66, far above the imposed limit of 0.32. The bacterial production measured in the top 3 mm was consistent with community respiration and was therefore used to solve the inverse model. This is extensively treated in the discussion.

The increasing use of available data resulted in differences among the CS, CIS and CITS and a large decrease in the uncertainty associated with these food webs. Main differences were found between the CS on the one hand and CIS and CITS on the other hand: 62 % of the flows in CIS and CITS differed more than $\pm$50 % from the CS (see 3.7 Appendix C). The large and small flows of the CIS and CITS agree well and differences mainly occur in flows of intermediate magnitude. The sum of carbon flows increased from 7670 (CS) to 8322 (CIS) to 8398 (CITS) mg C m^{-2} d^{-1}.

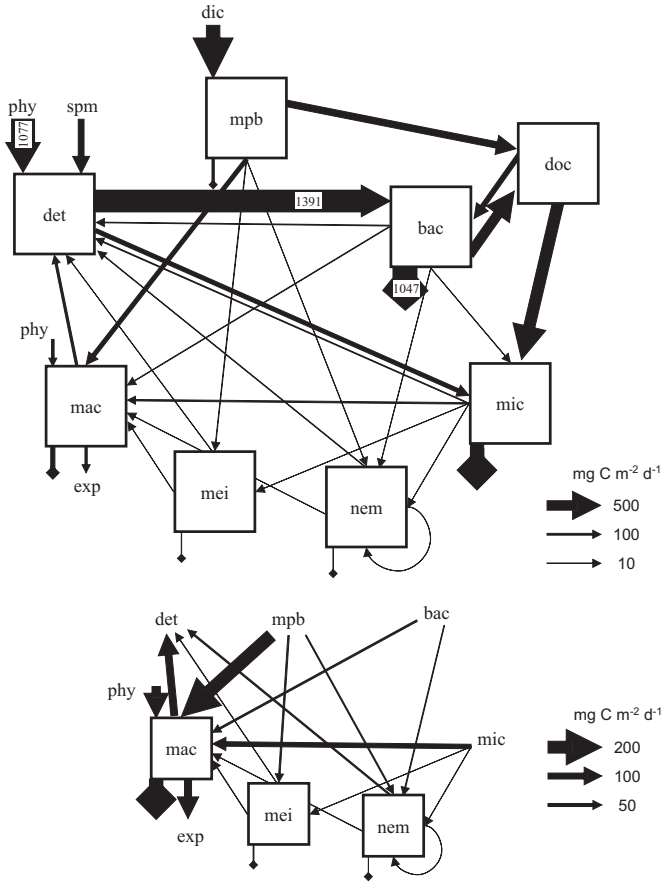

Figure 3.1: The inverse solution for the intertidal food web with flows based on assimilating biomass, stable isotope and tracer experiment data (CITS). Abbreviations: mpb is microphytobenthos, bac is bacteria, mic is microbenthos, nem is nematodes, mei is meiobenthos, mac is macrobenthos, doc is dissolved organic carbon, det is detritus, phy is phytoplankton, spm is suspended particulate matter, dic is dissolved inorganic carbon and exp is export from the system. Carbon inputs are primary production by microphytobenthos, macrobenthic suspension feeding on phytoplankton, phytoplankton and suspended particulate matter deposition. DOC is produced through EPS excretion by microphytobenthos and bacteria and consumed by bacteria and microbenthos. Detritus is consumed and produced (death and faeces production) by all heterotrophic compartments. Microphytobenthos and bacteria are grazed by microbenthos, nematodes, meiobenthos and macrobenthos. Microbenthos is grazed by nematodes, meiobenthos and macrobenthos, nematodes are grazed by predatory nematodes and macrobenthos, and meiobenthos is grazed by macrobenthos. Carbon outflows are respiration (diamond head arrows), macrobenthic export (e.g. consumption by fish or birds) and bacterial burial. Only non-zero flows are pictured. The arrows with indicated values are not scaled, because their dominance would otherwise mask the thickness differences among the other arrows. The lower panel shows nematodes, meiobenthos and macrobenthos on a different scale to better indicate the flow structure.

The uncertainty in CS is large: 51 % of the flows has a range of $>$ 500 mg C m^{-2} d^{-1} and 29 % a range of $>$ 1000 mg C m^{-2} d^{-1} (Table 3.2). The stable isotope data constrained the uncertainty significantly (Fig. 3.2): the ranges decreased $>$ 50 % for 60

% of the flows and $>$ 75 % for 34 % of the flows. In the CISrange, 25 % of the unknown flows still have a range larger than 200 mg C m^{-2} d^{-1}, but the range for $>$ 50 % of the flows is $<$ 70 mg C m^{-2} d^{-1}. The inclusion of the tracer data constrained some flows more than others (Fig. 3.2). The range of 37 % of the flows decreased $>$ 50 % as compared to the CISrange, in particular carbon flows related to microphytobenthos, nematodes and macrobenthos were better constrained in the CITSrange. The largest ranges in CITSrange are associated with phytoplankton deposition (between 799 and 1640 mg C m^{-2} d^{-1}), detritus uptake by bacteria (between 1314 and 1913 mg C m^{-2} d^{-1}) and the fate of ungrazed bacterial production (detritus, DOC or burial range between 0 and 570 mg C m^{-2} d^{-1}) (Table 3.2). In addition, flows associated with microbenthos have fairly large ranges: detritus and DOC ingestion by microbenthos have ranges of 555 and 495 mg C m^{-2} d^{-1}, respectively. Detritivorous flows are very well constrained for nematodes ($<$ 1 mg C m^{-2} d^{-1}), meiobenthos ($<$ 5 mg C m^{-2} d^{-1}) and macrobenthos ($<$ 40 mg C m^{-2} d^{-1}). Respiration fluxes are well constrained for nematodes (3 - 8 mg C m^{-2} d^{-1}), meiobenthos (13 - 60 mg C m^{-2} d^{-1}) and macrobenthos (226 - 323 mg C m^{-2} d^{-1}), but less for bacteria (993 - 1466 mg C m^{-2} d^{-1}) and microbenthos (290 - 763 mg C m^{-2} d^{-1}). Finally, EPS excretion by microphytobenthos is well constrained and is between 300 and 398 mg C m^{-2} d^{-1}.

The uncertainty in the tracer simulation based on the CISrange was large for microphytobenthos and bacteria, but particularly large for nematodes and macrobenthos (Fig. 3.3). The uncertainty in the tracer simulation based on CITSrange was smaller for all compartments, clearly demonstrating that the addition of tracer data further increased the reliability of the reconstructed food web. The optimal tracer simulation (CITS) describes the entire set of observations quite reasonably. The tracer dynamics of microphytobenthos fit the observations well, which means that the turnover time in our inverse solution is similar to that in the field. The food web model reproduces the quick tracer incorporation by bacteria and the peak labeling at 1-2 days. The modeled magnitude of nematode tracer incorporation is very similar to that observed in the field. However, the rapid initial enrichment is not reproduced and the modeled incorporation rate seems slightly higher than in the field. Macrobenthos tracer incorporation is somewhat overestimated as compared to the one field observation available.

Table 3.2: The intertidal benthic food web (CITS) and the associated uncertainty (CITSrange) (mg C m^{-2} d^{-1}). Flows in italics are field measurements and are therefore fixed in the solution. Abbreviations as in Fig. 3.1.

Flow	**CITS**	**CITSrange**	
		min	max
doc → bac	253	120	322
doc → mic	601	171	666
det → bac	1391	1314	1913
det → mic	210	0	555
det → nem	0	0	1
det → mei	0	0	5
det → mac	0	0	40
phy → det	1077	799	1640
phy → mac	139	139	218
spm → det	304	264	537
dic → mpb	*714*	*714*	*714*
mpb → dic	114	114	172

mpb → doc	348	300	398
mpb → det	0	0	52
mpb → mic	0	0	71
mpb → nem	17	17	64
mpb → mei	25	23	99
mpb → mac	210	155	258
bac → dic	1047	993	1466
bac → doc	506	0	571
bac → det	37	0	571
bac → mic	*13*	*13*	*13*
bac → nem	14	14	48
bac → mei	0	0	6
bac → mac	28	0	59
bac → bur	0	0	566
mic → dic	710	290	763
mic → det	38	0	86
mic → nem	0.4	0.4	5
mic → mei	2	0	8
mic → mac	75	62	156
nem → dic	3	3	8
nem → det	24	24	112
nem → nem	3	2	8
nem → mac	4	0	7
mei → dic	13	13	60
mei → det	6	6	43
mei → mac	8	8	23
mac → dic	226	226	323
mac → det	116	116	229
mac → exp	122	122	141

3.3.2 Carbon flows in the benthic food web

Bacteria dominate carbon flows at the Molenplaat and obtain 85 % of their carbon from detritus and the remainder from DOC (Fig. 3.1 and Table 3.2). DOC originates from microphytobenthic and bacterial EPS production and bacterial mortality. Bacteria assimilated 2122 mg C m^{-2} d^{-1} and their growth efficiencies on detritus and DOC were 0.32 and 0.63, respectively. Only 9 % of the total bacterial production is grazed and the majority of the production is recycled between DOC and bacteria. Microbenthos ingestion (825 mg C m^{-2} d^{-1}) is mostly DOC (73 %), supplemented with detritus (26 %) and bacteria (2 %). Nematode ingestion (35 mg C m^{-2} d^{-1}), comprises a small fraction of total heterotrophic ingestion (1 %). The main nematode food sources are microphytobenthos (50 %) and bacteria (39 %). Nematode predation forms 10 % of total nematode ingestion. The other meiobenthos (i.e. ostracods, copepods and foraminifera) play a marginal role in carbon cycling; the ingestion rate is restricted to 27 mg C m^{-2} d^{-1} (1 % of total heterotrophic ingestion), with dominant carbon sources being microphytobenthos (93 %) followed by microbenthos (7 %). As they have a high biomass, macrobenthos play an important role in carbon cycling and their ingestion is around 15 % of total heterotrophic ingestion. Important macrobenthic carbon sources are microphytobenthos (45 %) and

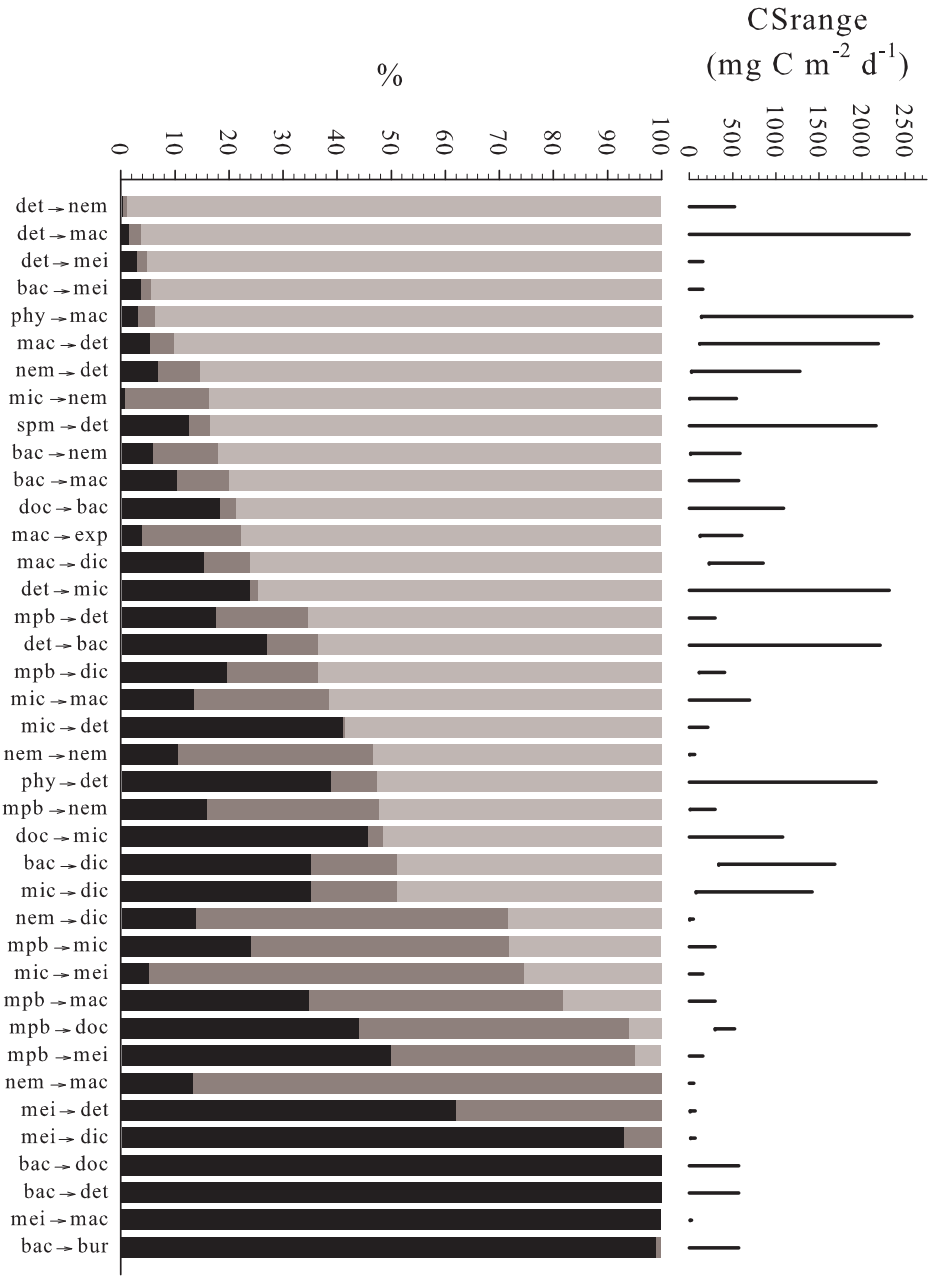

Figure 3.2: Absolute CSrange for each flow (upper panel) and the relative reduction of this CSrange (light grey) to CISrange (dark grey) to CITSrange (black) (lower panel). Abbreviations as in Fig. 3.1

phytoplankton (30 %). Ingestion of bacteria (6 %), microbenthos (16 %), nematodes (1 %) and meiobenthos (2 %) completes their diet. Surprisingly, the results show no ingestion of detritus by nematodes, meiobenthos nor macrobenthos.

The Molenplaat is heterotrophic and is supported by suspended particulate matter deposition (14 %), local primary production by microphytobenthos (32 %), suspension feeding by macrobenthos (6 %) and phytoplankton deposition (48 %) (Table 3.2). Respiration is dominated by bacterial respiration (50 %) with microbenthos as second contributor (34 %). The contribution of other compartments is smaller with 11 % for macrobenthos, 5 % for microphytobenthos and < 1 % for nematodes and meiobenthos (Table 3.2). Total secondary production amounts to 826 mg C m^{-2} d^{-1} and is again dominated by bacteria (74 %), followed by macrobenthos (15 %), microbenthos (10 %), nematodes (1 %) and other meiobenthos (1 %).

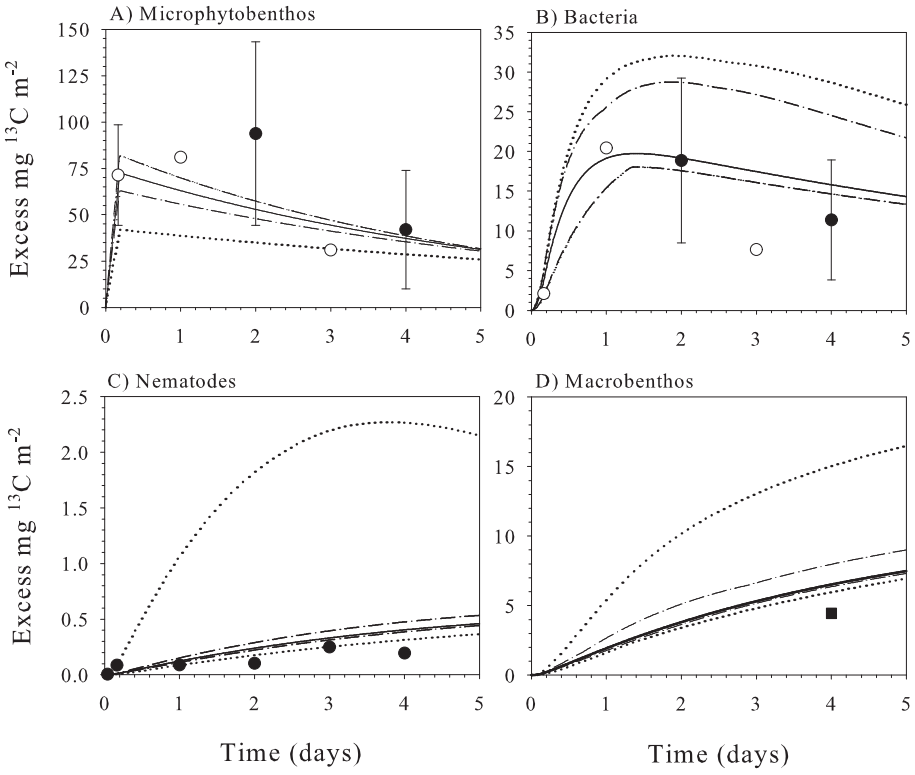

Figure 3.3: Tracer dynamics in the Molenplaat as measured in the top 5 mm (open circles), top 20 mm (filled circles) and top 20 cm (filled squares) and simulated based on the CITS (dark line). Also indicated are the range of tracer dynamics based on CISrange (dotted lines) and CITSrange (dashed dotted lines). The upper tracer dynamics ranges for CISrange and CITSrange overlap for microphytobenthos, while the lower ranges overlap for bacteria. When present, error bars denote standard deviations.

3.4 Discussion

The Molenplaat is one of the best-studied intertidal flats with comprehensive data on its physical, chemical and biological characteristics (Herman et al., 2001). Despite this extensive data set, producing a 'coherent and well-constrained' food web was ambiguous.

This ambiguity relates to data quality and availability and the inverse methodology. Hence, these will be discussed first, followed by a discussion on the importance of the herbivorous, detrital and microbial pathways in the benthic food web.

3.4.1 Field data

Spatial and temporal data acquisition

There is considerable heterogeneity in temporal and spatial sampling in the data set. The data have been collected in the period 1996 - 1999, some measurements were performed only once (e.g. δ^{13}C signatures and meiobenthic biomass), others are season-averaged (e.g. bacterial production, bacteria and microbenthos stock) and sampling depth ranged from 0-1 cm (meiobenthos) to 0-20 cm (macrobenthos). These temporal and spatial differences in data acquisition may partly explain some of the encountered discrepancies. However, several studies indicate no changes in microphytobenthic (Hamels et al., 1998), meiobenthic (M Steyaert, pers. com.) and macrobenthic (Herman et al., 2000) biomass and composition during the study period.

Bacterial production and community respiration

The inverse methodology identified the inconsistency between depth-integrated bacterial production (BP) and sediment community oxygen consumption (SCOC). Even when assuming that all respiration is bacterial, anomalously high growth efficiencies are needed. This inconsistency has frequently been reported in studies measuring both BP and SCOC (Van Duyl and Kop, 1990; Cammen, 1991; Alongi, 1995; Boon et al., 1998). Some potential problems with BP measurements are unbalanced growth and non-specificity or catabolism of the radioactive substrate that is added to measure BP (Kemp, 1990; Dixon and Turley, 2001). Moreover, BP is based on comparatively short incubations ($\sim$ 30 minutes). Compared to these uncertainties, SCOC measurements are more robust (Dauwe et al., 2001). SCOC integrates aerobic (direct oxygen consumption) and anaerobic (re-oxidation of reduced compounds) mineralization pathways over time scales in the order of days to weeks. The SCOC based on intact contact core incubations ranged from 1806 to 2406 mg C m^{-2} d^{-1} and compares well with independent community respiration measurements based on CO_2 production in slurry incubations ($\sim$ 2400 mg C m^{-2} d^{-1}) (Dauwe et al., 2001). As two different SCOC measures gave similar results and SCOC integrates heterotrophic activity over a longer time scale than BP measurements, it is therefore taken as the most appropriate measure to constrain total benthic activity at the expense of the depth integrated BP. In addition, a long-term ^{13}C-glucose labeling experiment yielded a BP of 798 mg C m^{-2} d^{-1} in the top 10 cm of the sediment (Chapter 4), which compares favorably to the BP adopted here (598 mg C m^{-2} d^{-1}).

Bacterial δ^{13}C signature

Measuring the bacterial δ^{13}C poses difficulties as this can only be assessed using bacterial specific biomarkers as proxy (Boschker and Middelburg, 2002). A critical assumption is that the isotope signature of such specific fatty acids (PLFAs) reflects that of bacterial biomass. Hayes (2001) reviews the results of *Escherichia coli* culture studies and finds a depletion of PLFAs as compared to total biomass of 3 to 8 ‰. A similar depletion has been found in culture studies using an inoculate of a natural bacterial community (Boschker et al., 1999). Whether these results may be translated to the field is unclear (Bouillon et al.,

2004), as fractionation depends amongst others on the relative abundance of lipids (Hayes, 2001), substrate utilization (DeNiro and Epstein, 1977) and oxygen concentration (Teece et al., 1999). For microbial substrate use in soils, it has been suggested that their is no depletion of PLFAs with respect to the substrate and that therefore the average δ^{13}C of different PLFAs is a good indicator of the δ^{13}C of the microbial substrate (Burke et al., 2003). Here, we choose for the latter approach for two reasons. First, assuming a typical depletion of 5 ‰ would lead to a bacterial δ^{13}C of -14.5 ‰, which could not be resolved with respect to the other observations. Second, such heavy bacterial δ^{13}C values would point to microphytobenthos as the dominant carbon source for bacteria. This is unlikely as (1) bacterial respiration outbalances microphytobenthos production and (2) the δ^{13}C of bacterial biomarkers did not show a depth gradient.

3.4.2 Extended inverse methodology, stable isotopes and tracer data

Food web studies taking a quantitative ecosystem perspective have revealed important insights in the structure of natural food webs (Lindeman, 1942; De Ruiter et al., 1995; Pauly et al., 1998; Gaedke et al., 2002) and inverse models are increasingly used to quantify food webs. However, a major problem is that a unique solution is selected by a parsimonious criterium (Vézina and Platt, 1988) or by upgrading site-specific data with literature data (Chapter 2). The methodology presented here, aims to increase the amount of site-specific data by additionally incorporating stable isotope and tracer data. The incorporation of the tracer data made the parsimonious criterium redundant, since the inverse solution with an optimal fit to the tracer data was chosen rather than the parsimonious solution.

Mixing models have become standards in ecology to estimate trophic position (Minagawa and Wada, 1984; Vander Zanden and Rasmussen, 1999) or diet contribution of $x + 1$ resources from x different isotopes (Peterson et al., 1986; Fry, 1991; Herman et al., 2000; Phillips, 2001; Post, 2002). When more than $x + 1$ resources are available to a consumer, it is impossible to uniquely estimate the resource diet contributions based on x different isotopes. For such situations, Phillips and Gregg (2003) propose a grid search technique to estimate a feasible range and frequency distribution for the contributions of different resources, rather than calculating a unique solution. In our study we similarly take advantage of a grid search technique (Appendix B), but use data on total carbon processing as additional constraints. This serves two purposes. First, while previous isotope applications have been very fruitful in quantifying the *relative* trophic position or *relative* contribution of a resource, we also quantify the absolute magnitude of all food web flows. Two, combining stable isotope and total carbon processing data increases the data resolution such that the uncertainty in the food web reconstruction decreases.

The integration of tracer experiments and modeling has proven to provide quantitative insight in food web interactions (Cole et al., 2002; Van den Meersche et al., 2004). Although the data from the tracer experiment provided quantitative information on the transfer of recently fixed carbon (Middelburg et al., 2000), sampling in itself was insufficient to quantify all food web flows. Instead, a tracer model was used to identify the inverse solution that optimally reproduced these tracer data. In general, the correspondence between model and data is acceptable (Fig. 3.3). The correspondence for microphytobenthos suggests that its turnover time and the fraction of the primary production excreted as EPS are accurately modeled. The general data - model agreement for bacteria gives credit to our previously discussed assumptions regarding bacterial

production and bacterial δ^{13}C. Although the magnitude of nematode labeling is reproduced by the model, the initial incorporation lags slightly behind the observations. This may be explained by ingestion of DOC (not modeled) or selective ingestion of active, highly labeled microphytobenthos cells.

Modeled macrobenthic label incorporation was overestimated by a factor 1.5, as compared to the one observation. Several explanations for this discrepancy may apply. First, due to the limited spatial scale of the experiment, 30 % of the deposit feeders (e.g. *Arenicola marina*) were not present in the samples from the tracer experiment and their label incorporation could not be assessed. Second, only 19 % of the deposit feeders classify as surface deposit feeders and had access to the highly labeled microphytobenthos in the top layer of the sediment. An implicit assumption in the tracer model is that the total deposit feeding community has direct access to the labeled microphytobenthos and therefore the model likely overestimates label incorporation. As there is only one observation and several plausible explanations for an overestimation of modeled label incorporation, we feel that the discrepancy is not strong enough to question the results.

The addition of stable isotope and tracer data changed the solutions, 62 % of the flows in CIS and CITS differed more than $\pm$ 50 % from the CS. The sum of carbon flows increased from 7670 (CS) to 8322 (CIS) to 8398 (CITS) mg C m^{-2} d^{-1}, corroborating the results from twin-modeling that show underestimation of flows in the parsimonious solution in recycling webs (Vézina and Pahlow, 2003). Moreover, inclusion of tracer data in the inverse solution made the parsimonious criterium redundant. The CITS food web is therefore free from the bias known to be introduced by such a criterium (Niquil et al., 1998). Finally, the integration of biomass, process, stable isotope and tracer data significantly reduced the uncertainty in the food web.

3.4.3 Pathways in the benthic food web

The biomass of bacteria, microbenthos, meiobenthos and macrobenthos for the Molenplaat can be considered representative for temperate estuarine tidal flats (Epstein and Shiaris, 1992; Heip et al., 1995; Soetaert et al., 1995; Herman et al., 1999). This also holds for bacterial production (Van Duyl and Kop, 1990), primary production and sediment oxygen consumption (Heip et al., 1995). Accordingly, the food web structure and functioning can be generalized and in this last section we discuss the importance of the herbivorous, detrital and microbial pathways.

Herbivorous pathway. The primary producers microphytobenthos and phytoplankton supported nematodes, other meiobenthos and macrobenthos in this heterotrophic benthic food web. Recent studies of food webs in estuaries (Thompson and Schaffner, 2001; Sobczak et al., 2002; Chanton and Lewis, 2002), streams (Tank et al., 2000) and lakes (Cole et al., 2002) report a similar dominant contribution of autochthonous production in diets of metazoan grazers. These results suggest that the algal-grazer link is the most important food web interaction to consider for higher trophic levels.

Microphytobenthos excrete 49 % of their carbon production as EPS, which enters the microbial pathway as dissolved organic carbon.

Microbial pathway. Bacteria dominate carbon flows and account for 74 % of secondary production and 50 % of respiration. This agrees with earlier reports on the bacterial dominance of production (Schwinghamer et al., 1986; Chardy and Dauvin, 1992) and respiration (Smith, 1973; Schwinghamer et al., 1986; Moodley et al., 2002). Grazing by higher trophic levels on bacteria is restricted and therefore bacterial production is a sink rather than a link of carbon in the benthic food web. Short-term bacterivory

studies of micro-, meio- or macrobenthos report similar limited transfer of bacterial carbon production (Kemp, 1987; Epstein and Shiaris, 1992; Hondeveld et al., 1995; Epstein, 1997a). The fate of bacterial production, other than grazing, was poorly constrained in this food web. Bacterial carbon might be recycled back to DOC or detritus or buried in the sediment. Several papers indicate that bacterial biomass and production rates are closely coupled to the distribution of viruses (e.g. Paul et al., 1993; Fischer et al., 2003) and viral lysis of bacterial cells might explain the recycling fluxes to the abiotic compartments. Although burial of recalcitrant bacterial cell-wall remnants is observed in ocean margin sediments (Parkes et al., 1993; Grutters et al., 2002), it is unknown whether this is a quantitatively important sink of bacterial production.

Microbenthos has a comparatively high carbon demand due to their high specific production and low growth efficiency. Their low rate of bacterivory implies that bacteria constitute 2 to 3 % of their diet. This is surprisingly low, given that microbenthos biomass at this study site is dominated by flagellates, which are typically seen as bacterivores. Consequently, either other carbon sources form their main food source or reported production rates are overestimates for field situations. The contribution of other resources (microphytobenthos, detritus and DOC) are poorly constrained, but DOC seems to form an important resource for microbenthos. Although flagellates are known for their capability to use dissolved organic substances (Sherr, 1988), its significance in sediments remains to be established. In the Molenplaat food web, microbenthos carbon production was transferred higher up the food web (Fig. 3.1). Hamels et al. (2001a) found evidence for such a transfer in laboratory incubations, in which nematodes heavily grazed ciliates. Hence, the microbial loop seems to have a dead end in bacteria, but there is potential transfer of DOC through microbenthos to higher trophic levels.

Detrital pathway. Semi-labile detritus supported the majority of bacterial carbon production and some of the microbenthos production. The rapid transfer of tracer to bacteria observed in the labeling experiment is fully explained by labile EPS excretion by microphytobenthos and subsequent assimilation by bacteria. However, DOC represents only 15 % of the total bacterial carbon demand. The importance of semi-labile detritus for bacterial production found in this intertidal flat food web can be explained from a biogeochemical viewpoint. Oxygen is rapidly consumed in the top millimeters of coastal sediments. Detritus is therefore predominantly degraded in the bacterial domain of suboxic and anoxic metabolic pathways (e.g. Canfield et al., 1993). Moreover, the labile part of detritus is degraded in the top layer of the sediment and therefore the most likely bacterial resource under suboxic/anoxic is semi-labile detritus.

Although the intertidal flat food web supports a large population of deposit feeding nematodes, meiobenthos and macrobenthos, these organisms appear to selectively assimilate high quality resources such as microphytobenthos, phytoplankton and to a lesser extent bacteria. Selective assimilation of high quality carbon has been demonstrated directly using δ^{13}C labeled phytodetritus (Blair et al., 1996; Levin et al., 1999; Herman et al., 2000; Moodley et al., 2002; Witte et al., 2003). This high selectivity suggests that bulk organic matter is a poor indicator of resource availability for deposit feeding organisms and refined descriptions, based on organic matter quality, are required for estimates of food availability.

The conceptual model of Mayer et al. (2001) is especially interesting when trying to explain the observed resource partitioning between bacteria and higher organisms. They relate digestive differences between deposit feeders (digestive tract) and bacteria (extra-cellular enzymes) to resource quality and suggest that deposit feeders benefit from high quality resources and that bacteria can better handle low quality resources. Their

predictions match the general picture that emerges for this intertidal food web. Whether their concept is indeed the mechanism that explains our results is an intriguing, yet open, question.

In summary, we find two major food web pathways in our intertidal flat with comparatively limited interaction. The semi-labile detrital pathway dominates carbon flows in the food web and supports the majority of the bacterial secondary production. Transfer of bacterial carbon to higher trophic levels is very restricted and instead recycles back to detritus and DOC. The herbivorous pathway is the second dominant pathway, in which microphytobenthos and phytoplankton supply labile carbon to the food web. Nematodes, meiobenthos and macrobenthos feed selectively on this particulate carbon production. Although many species in these benthos groups classify as deposit feeder, this selectivity results in a virtual absence of detritivory. The observed separation of carbon pathways suggests that they function rather autonomously.

3.5 Appendix A: Inverse model equality and constraint equations

This appendix contains all inverse model equations (Table 3.3) and constraints (Table 3.4) with references. Some equations and constraints require additional explanation, which is given below.

Bacterial growth efficiency (BGE) varies considerably among carbon sources (del Giorgio and Cole, 1998). Therefore different BGE for growth on detritus ($BGEdet$) and DOC ($BGEdoc$) are assumed, however, with the restriction that $BGEdoc$ is two times $BGEdet$. The BGE ranges for growth on DOC and detritus in a comprehensive literature review indeed show such a pattern (del Giorgio and Cole, 1998). This pattern is consistent with the notion that detritus uptake is a two-step process: 1) detritus dissolution and 2) subsequent assimilation, whereas DOC uptake only involves the second step. The ratio $BGEdoc$ to $BGEdet$ is fixed to two in order to reduce the number of free parameters in the grid search from 4 to 3 (see Appendix B). This saves considerably on the required calculations in the grid search, while still being a good approximation of reality.

The respiration flows for microbenthos, nematodes, meiobenthos and macrobenthos are described as the sum of two processes: maintenance and growth respiration. Maintenance costs are taken proportional to biomass (Table 3.3). It is often found that respiration rates in starved heterotrophic organisms drop to less than a few percent of their biomass per day (Fenchel, 1982; Kristensen, 1989; Nielsen et al., 1995), hence the specific maintenance respiration is fixed to 1 % of the biomass per day. Respiration costs related to growth processes can be considerably higher and are modeled as a fixed fraction of assimilated carbon. This fraction equals $1 - NGE$, with NGE being the net growth efficiency.

Table 3.3: Inverse model equations. Abbreviations: mpb is microphytobenthos, bac is bacteria, mic is microbenthos, nem is nematodes, mei is meiobenthos, mac is macrobenthos, doc is dissolved organic carbon, det is detritus, dic is dissolved inorganic carbon, phy is phytoplankton, spm is suspended particulate matter, exp is export and bur is burial. All mass balances are assumed to be in steady state. Flows are designated as $source \rightarrow sink$.

Mass balances
$\frac{d\ mpb}{d\ t} = 0 = dic \rightarrow mpb - mpb \rightarrow dic - mpb \rightarrow doc - mpb \rightarrow det$
$-mpb \rightarrow mic - mpb \rightarrow nem - mpb \rightarrow mei - mpb \rightarrow mac$
$\frac{d\ bac}{d\ t} = 0 = doc \rightarrow bac + det \rightarrow bac - bac \rightarrow dic - bac \rightarrow doc$
$-bac \rightarrow det - bac \rightarrow bur - bac \rightarrow mic - bac \rightarrow nem$
$-bac \rightarrow mei - bac \rightarrow mac$
$\frac{d\ mic}{d\ t} = 0 = mpb \rightarrow mic + bac \rightarrow mic + doc \rightarrow mic + det \rightarrow mic$
$-mic \rightarrow dic - mic \rightarrow det - mic \rightarrow nem$
$-mic \rightarrow mei - mic \rightarrow mac$
$\frac{d\ nem}{d\ t} = 0 = mpb \rightarrow nem + bac \rightarrow nem + mic \rightarrow nem + det \rightarrow nem$
$-nem \rightarrow dic - nem \rightarrow det - nem \rightarrow mac$
$\frac{d\ mei}{d\ t} = 0 = mpb \rightarrow mei + bac \rightarrow mei + mic \rightarrow mei$
$+det \rightarrow mei - mei \rightarrow dic - mei \rightarrow det - mei \rightarrow mac$
$\frac{d\ mac}{d\ t} = 0 = mpb \rightarrow mac + bac \rightarrow mac + mic \rightarrow mac + nem \rightarrow mac$
$+mei \rightarrow mac + det \rightarrow mac + phy \rightarrow mac$
$-mac \rightarrow dic - mac \rightarrow exp$
$\frac{d\ doc}{d\ t} = 0 = mpb \rightarrow doc + bac \rightarrow doc - doc \rightarrow bac - doc \rightarrow mic$

$$\frac{d\,det}{d\,t} = 0 = phy \rightarrow det + spm \rightarrow det + mpb \rightarrow det + bac \rightarrow det$$
$$+mic \rightarrow det + nem \rightarrow det + mei \rightarrow det + mac \rightarrow det$$
$$-det \rightarrow bac - det \rightarrow mic - det \rightarrow nem$$
$$-det \rightarrow mei - det \rightarrow mac$$

Isotope mass balances

$$\delta^{13}C\text{-}bac = \frac{BGEdoc \cdot doc \rightarrow bac}{BGEdoc \cdot doc \rightarrow bac + BGEdet \cdot det \rightarrow bac} \cdot \delta^{13}C\text{-}doc + \frac{BGEdet \cdot det \rightarrow bac}{BGEdoc \cdot doc \rightarrow bac + BGEdet \cdot det \rightarrow bac} \cdot \delta^{13}C\text{-}det$$

$$\delta^{13}C\text{-}mic = \frac{doc \rightarrow mic}{doc \rightarrow mic + det \rightarrow mic + mpb \rightarrow mic + bac \rightarrow mic} \cdot \delta^{13}C\text{-}doc + \frac{det \rightarrow mic}{doc \rightarrow mic + det \rightarrow mic + mpb \rightarrow mic + bac \rightarrow mic} \cdot \delta^{13}C\text{-}det + \frac{mpb \rightarrow mic}{doc \rightarrow mic + det \rightarrow mic + mpb \rightarrow mic + bac \rightarrow mic} \cdot \delta^{13}C\text{-}mpb + \frac{bac \rightarrow mic}{doc \rightarrow mic + det \rightarrow mic + mpb \rightarrow mic + bac \rightarrow mic} \cdot \delta^{13}C\text{-}bac$$

$$\delta^{13}C\text{-}nem = \frac{det \rightarrow nem}{det \rightarrow nem + mpb \rightarrow nem + bac \rightarrow nem + mic \rightarrow nem} \cdot \delta^{13}C\text{-}det + \frac{mpb \rightarrow nem}{det \rightarrow nem + mpb \rightarrow nem + bac \rightarrow nem + mic \rightarrow nem} \cdot \delta^{13}C\text{-}mpb + \frac{bac \rightarrow nem}{det \rightarrow nem + mpb \rightarrow nem + bac \rightarrow nem + mic \rightarrow nem} \cdot \delta^{13}C\text{-}bac + \frac{mic \rightarrow nem}{det \rightarrow nem + mpb \rightarrow nem + bac \rightarrow nem + mic \rightarrow nem} \cdot \delta^{13}C\text{-}mic$$

$$\delta^{13}C\text{-}mei = \frac{det \rightarrow mei}{det \rightarrow mei + mpb \rightarrow mei + bac \rightarrow mei + mic \rightarrow mei} \cdot \delta^{13}C\text{-}det + \frac{mpb \rightarrow mei}{det \rightarrow mei + mpb \rightarrow mei + bac \rightarrow mei + mic \rightarrow mei} \cdot \delta^{13}C\text{-}mpb + \frac{bac \rightarrow mei}{det \rightarrow mei + mpb \rightarrow mei + bac \rightarrow mei + mic \rightarrow mei} \cdot \delta^{13}C\text{-}bac + \frac{mic \rightarrow mei}{det \rightarrow mei + mpb \rightarrow mei + bac \rightarrow mei + mic \rightarrow mei} \cdot \delta^{13}C\text{-}mic$$

$$\delta^{13}C\text{-}mac = \frac{det \rightarrow mac}{\sum inflow} \cdot \delta^{13}C\text{-}det + \frac{phy \rightarrow mac}{\sum inflow} \cdot \delta^{13}C\text{-}phy + \frac{mpb \rightarrow mac}{\sum inflow} \cdot \delta^{13}C\text{-}mpb + \frac{bac \rightarrow mac}{\sum inflow} \cdot \delta^{13}C\text{-}bac + \frac{mic \rightarrow mac}{\sum inflow} \cdot \delta^{13}C\text{-}mic + \frac{nem \rightarrow mac}{\sum inflow} \cdot \delta^{13}C\text{-}nem + \frac{mei \rightarrow mac}{\sum inflow} \cdot \delta^{13}C\text{-}mei$$

with $\sum inflow = det \rightarrow mac + phy \rightarrow mac + mpb \rightarrow mac$
$+bac \rightarrow mac + mic \rightarrow mac + nem \rightarrow mac + mei \rightarrow mac$

Equations

Gross primary production	$dic \rightarrow mpb = 714$
Bacterivory by microbenthos	$bac \rightarrow mic = 12.8$
Sediment respiration	$mpb \rightarrow dic + bac \rightarrow dic + mic \rightarrow dic$ $+nem \rightarrow dic + mei \rightarrow dic + mac \rightarrow dic = 2112$
Bacterial growth efficiency	$BGEdoc = 2 \cdot BGEdet$
Bacterial production	$BGEdet \cdot det \rightarrow bac+$ $BGEdoc \cdot doc \rightarrow bac = 598$
Maintenance respiration	$0.01 \cdot biomass$

Table 3.4: Constraints imposed on the benthic food web. Sources are 1) Langdon (1993), 2) Goto et al. (1999), 3) del Giorgio and Cole (1998), 4) Toolan (2001), 5) Verity (1985), 6) Zubkov and Sleigh (1999), 7) Wieltschnig et al. (2001), 8) Capriulo (1990), 9) Fenchel (1982), 10) Straile (1997), 11) Sleigh and Zubkov (1998), 12) Anderson (1992), 13) Herman and Vranken (1988), 14) Heip et al. (1985), 15) Woombs and Laybourn-Parry (1985), 16) Woombs and Laybourn-Parry (1984), 17) Gerlach (1971), 18) Schiemer (1982), 19) Schiemer et al. (1980), 20) Vranken and Heip (1986), 21) Vranken et al. (1986), 22) Heip et al. (1982), 23) Schiemer (1983), 24) Moens and Vincx (1997), 25) Landry et al. (1983), 26) Conover (1966), 27) Cowie and Hedges (1996), 28) Fleeger and Palmer (1982), 29) Feller (1982), 30) Ceccherelli and Mistri (1991), 31) Herman and Heip (1985), 32) Banse and Mosher (1980), 33) Herman et al. (1983), 34) Ikeda et al. (2001), 35) Vidal (1980), 36) Herman et al. (1984), 37) Nielsen et al. (1995), 38) Kristensen (1989), 39) Arifin and Bendell-Young (2001), 40) Hummel et al. (2000), 41) Loo and Rosenberg (1996), 42) Lopez and Cheng (1983), 43) Arifin and Bendell-Young (1997), 44) Lopez and Levinton (1987), 45) Jordana et al. (2001), 46) Sprung (1993), 47) Heip et al. (1995), 48) Thompson and Schaffner (2001), 49) Robertson (1979), 50) Vedel and Riisgård (1993), 51) Calow (1977).

Process	Flow/units	Lower boundary	Upper boundary	Sources
Microphytobenthos				
Respiration	$mpb \rightarrow dic$	$0.16 \cdot dic \rightarrow mpb$		[1]
Excretion	$mpb \rightarrow doc$	$0.42 \cdot dic \rightarrow mpb$	$0.73 \cdot dic \rightarrow mpb$	[2]
Bacteria				
$BGEdet$[a]	-	0.06	0.32	[3,4]
Microbenthos				
AE[b]	-	0.91	1.0	[5]
PB[c]	d^{-1}	0.50	5.0	[6–9]
NGE[d,e]	-	0.10	0.50	[6,10–12]
Nematodes				
AE[b]	-	0.06	0.30	[13–16]
PB[c]	d^{-1}	0.05	0.40	[13,15,17–22]
NGE[d]	-	0.60	0.90	[13–15,23]
Bacterivory[f]	$bac \rightarrow nem$	$\frac{bac}{bac+mic}\frac{nem_{mic}}{nem}C_{nem}$		[24]
Microbenthos[f]	$mic \rightarrow nem$	$\frac{mic}{bac+mic}\frac{nem_{mic}}{nem}C_{nem}$		[24]
Herbivory[f]	$mpb \rightarrow nem$	$\frac{nem_{epi}}{nem}C_{nem}$		[24]
Predation[f]	$nem \rightarrow nem$	$\frac{nem_{pre}}{nem}C_{nem}$	$\frac{nem_{pre}+nem_{fac}}{nem}C_{nem}$	[24]
Meiobenthos				
AE[b]	-	0.57	0.77	[25–27]
PB[c]	d^{-1}	0.03	0.09	[28–33]
NGE[d]	-	0.30	0.50	[31–36]
Macrobenthos				
AE[b]	-	0.40	0.75	[41–45]
PB[c]	d^{-1}	0.01	0.05	[37,41,46–50]
NGE[d]	-	0.50	0.70	[37,51]
Phytoplankton[g]	$phy \rightarrow mac$	$\frac{mac_{sus}}{mac}C_{mac}$		

[a] The range of $BGEdet$ is determined from the range of values for seaweeds (del Giorgio and Cole, 1998), this range covers the range in BGE for phytoplankton and faeces as well.

[b] AE is assimilation efficiency and is defined as $\frac{\sum inflow - loss\ to\ detritus}{\sum inflow}$.

[c] PB is production to biomass ratio.

[d] NGE is net growth efficiency and is defined as $\frac{\sum inflow - loss\ to\ detritus - respiration}{\sum inflow - loss\ to\ detritus}$.
[e] data on gross growth efficiency (GGE) are the quartiles of the box-whisker plot for flagellates and ciliates in Straile (1997), i.e. 10 % and 45 %. Subsequently net growth efficiency is calculated as $NGE = \frac{GGE}{AE}$.
[f] bac is bacterial biomass, mic is microbenthos biomass, nem_{mic} is the biomass of the nematode feeding groups microvores and ciliate feeders, nem_{epi} is the biomass of the nematode epistrate feeding group, nem_{pre} is the biomass of the nematode predator feeding group, nem_{fac} is the biomass of the nematode facultative predator feeding group, nem is nematode biomass and C_{nem} is the total consumption by nematodes.
[g] mac_{sus} is the biomass of the macrobenthos suspension feeding group, mac is the macrobenthos biomass and C_{mac} is the total consumption by macrobenthos.

3.6 Appendix B: Introducing stable isotope and tracer data in an inverse model

3.6.1 Stable isotope data

First it is detailed how isotope mass balances are set up in the inverse model. Mixing models require that isotope data of all components are available, which is generally not the case in complex food webs. Second, we therefore explain how a grid search can be used in case some isotope signatures are lacking. Finally, we describe the method to assimilate tracer data in the food web reconstruction.

Isotope mass balances

Isotope signatures are commonly expressed in the delta notation, which is a ‰ deviation from a reference material

$$\delta^h I = \frac{\left(\frac{^hI}{^lI}\right)_{sample} - \left(\frac{^hI}{^lI}\right)_{reference}}{\left(\frac{^hI}{^lI}\right)_{reference}} \cdot 1000 \tag{3.4}$$

where $\frac{^hI}{^lI}$ is ratio of the heavy isotope (^hI, e.g. ^{13}C, ^{15}N or ^{34}S) to the more common and lighter isotope (^lI, e.g. ^{12}C, ^{14}N or ^{32}S) in the sample and reference material.

The common formulation of an isotope mixing model for a consumer that feeds on n resources is

$$\delta^h I_j = \sum_{i=1}^{n} (\delta^h I_i + \Delta_i) \cdot \alpha_i \tag{3.5}$$

where $\delta^h I_j$ is the isotope signature of consumer j, $\delta^h I_i$ is the isotope signature of resource i, Δ_i is the fractionation factor and α_i is the relative contribution of resource i in the diet of consumer j. Necessarily, the relative diet contributions sum to 1, i.e. $\sum_{i=1}^{n} \alpha_i = 1$.

This mixing model is easily extended to a form that includes the flows as unknowns. For this, the relative contribution resource is defined as

$$\alpha_i = \frac{flow_{i \to j} \cdot \varepsilon_i}{\sum_{i=1}^{n} flow_{i \to j} \cdot \varepsilon_i} \tag{3.6}$$

where $flow_{i \to j}$ is the flow of resource i to consumer j and ε_i is the incorporation efficiency of resource i into the biomass of consumer j. With this definition, the linear mixing model becomes a function of the food web flows as

$$\delta^h I_j \cdot \sum_{i=1}^{n} (flow_{i \to j} \cdot \varepsilon_i) = \sum_{i=1}^{n} \left(\left(\delta^h I_i + \Delta_i \right) \cdot flow_{i \to j} \cdot \varepsilon_i \right) \tag{3.7}$$

Note that when the growth efficiency (ε_i) is taken equal for the different resources, it drops from the equation. As this equation is a linear expression of the food web flows, it is easily appended to the equality equations of the inverse model (see Table 3.3).

Dealing with unknown isotope values

From the isotope mass balance description it is clear that the isotope composition of all resources are required and the growth efficiencies for each food source should either be the same or known. For the Molenplaat case study there were four unknown parameters: δ^{13}C-microbenthos, δ^{13}C-DOC, $BGEdet$ and $BGEdoc$. This number was reduced to three by assuming $BGEdoc = 2 \cdot BGEdet$ (see Appendix A for justification). To overcome these data deficiencies we developed approach based on a grid search. This method resembles the approach proposed by Phillips and Gregg (2003), who used a grid search to estimate the importance of different resources for a consumer, in case no unique solution could be found.

First, the potential range of each parameter was determined. The range on bacterial growth efficiency on detritus was taken from the literature (0.06 - 0.32, see Appendix A). The isotope signatures ranges were taken from the available isotope signatures of other compartments. From the food web structure, all the potential resource compartments were identified and the minimal and maximal isotope signatures from the resources were selected. The possible sources for DOC are bacteria (δ^{13}C of -20.4) and microphytobenthos (δ^{13}C of -15.0). Hence, the δ^{13}C-DOC should lie between -20.4 and -15.0. The end members for microbenthos in terms of their isotope signature are detritus (δ^{13}C of -21.2) and microphytobenthos (δ^{13}C of -15.0).

The ranges of these three parameters span a 3 dimensional space of all possible combinations. These initial ranges are not yet affected by the information implemented in the inverse model. To delineate the combinations of isotope signatures that are compatible with the other inverse model equations and constraints, we performed a grid search. Each parameter range was discretized (step size for isotopes 0.10 and for BGE 0.05) on a grid and the inverse model solved for every parameter combination. When the other data in the inverse model are not compatible with a certain parameter combination, the model residuals are not zero (i.e. the model cannot be solved without deviation from the imposed data). The model residual was calculated as the deviation from the linear equality and inequality equations

$$Residual\ norm = (\mathbf{Ax} - \mathbf{b})^T(\mathbf{Ax} - \mathbf{b}) + (\mathbf{Gx} - \mathbf{h})^T\Gamma(\mathbf{Gx} - \mathbf{h}) \tag{3.8}$$

Γ is a diagonal matrix whose diagonal elements are unity when the argument is negative, and zero when the argument is positive

$$\Gamma_{i,i} = \begin{cases} 0, & (\mathbf{Gx} - \mathbf{h})_i \geq 0 \\ 1, & (\mathbf{Gx} - \mathbf{h})_i < 0 \end{cases} \tag{3.9}$$

This ensures that only the inequalities that are violated add to the residual norm. By performing this evaluation for each possible parameter combination, one can delineate the possible parameter combinations that are compatible with the other data. The parameter combination that has a zero residual norm and is minimal in $\sum_{i=1}^{n} x_i^2$, is the simplest or parsimonious food web (sensu Vézina and Platt (1988)).

3.6.2 Tracer data

The output of an inverse model is a food web in which all flows are quantified. These flow values, in combination with the stock size of the compartments, determine how a tracer flows through the food web. The inverse food web model with conventional and stable isotope data is an under determined system. This implies that, within the limits set

by these data, there is an infinite amount of different food webs that all satisfy these data equally well. Put otherwise, there is no one unique solution that optimally reproduces the data in the inverse model, but an infinite amount. However, each food web has different flow values and will therefore differ in the way a tracer flows through it. In the final step of quantifying the intertidal food web, we aim to find the food web whose tracer dynamics optimally resemble the observations from the tracer experiment.

First, the inverse model, with conventional and isotope data, was repeatedly solved and during each run the minimization function that weighted the different flows was varied

$$J = \sum_{i=1}^{n} w_i \; {x_i}^2 \tag{3.10}$$

where $\mathbf{w}$ contains n weighting factors (Lawson and Hanson, 1995). The elements of $\mathbf{w}$ were randomly varied between 1 and 100 for each run (when $\mathbf{w} = 1$ this corresponds to finding the parsimonious solution). As the contribution of a flow in the minimization function differed with each run, numerous different inverse solutions were generated (618393 in this case for practical reasons). These generated inverse solutions covered > 91 % of the CISrange of all flows, except for the flows microbenthos to nematodes (84 % covered) and microbenthos to meiobenthos (73 % covered) (data not shown). This means that each flow range (CISrange) was sufficiently covered in our attempt to find the food web that optimally reproduces the tracer data.

Second, a tracer model was set up to simulate tracer flow through each food web. A specific rate constant ($\tau_{i\rightarrow j}$, d^{-1}) was calculated for each flow

$$\tau_{i\rightarrow j} = \frac{flow_{i\rightarrow j}}{stock_i} \tag{3.11}$$

in which $flow_{i\rightarrow j}$ is the flow from compartment i to j and $stock_i$ is the stock size of compartment i. These rate constants were used to set up the tracer model (Table 3.5). In the tracer model the processes respiration, excretion and faeces production have a tracer concentration equal to that of the incoming flows. Other outgoing flows, i.e. grazing, predation or export have the tracer concentration of the biotic compartment (Table 3.5). To initialize the tracer simulation, the incorporation rate of ^{13}C-HCO_3^- into microphytobenthos was set to the observed fixation rate of 32 mg ^{13}C m^{-2} h^{-1} during a period of 4.5 hours. The model was solved in the modeling environment FEMME (Soetaert et al., 2002) and can be downloaded from http://www.nioo.knaw.nl/ceme/femme.

Table 3.5: Model equations of the dynamic tracer model. FixRate is the observed fixation rate of microphytobenthos (32 mg ^{13}C m^{-2} h^{-1} during 4.5 hours). The tracer concentration in a compartment is denoted as $stock^{tr}$. Abbreviations as in Fig. 3.1

$\tau_{i\rightarrow j} = \frac{flow_{i\rightarrow j}}{stock_i}$
$\frac{d\ mpb^{tr}}{d\ t} = \Gamma \cdot FixRate \cdot (1 - \frac{mpb\rightarrow doc + mpb\rightarrow dic}{dic\rightarrow mpb})$
$-mpb^{tr} \cdot (\tau_{mpb\rightarrow det} + \tau_{mpb\rightarrow mic} + \tau_{mpb\rightarrow nem} + \tau_{mpb\rightarrow mei} + \tau_{mpb\rightarrow mac})$
with $\Gamma = \begin{cases} 0, & t > \frac{4.5}{24} \\ 1, & t \leq \frac{4.5}{24} \end{cases}$
$\frac{d\ bac^{tr}}{d\ t} = BGEdoc \cdot doc^{tr} \cdot \tau_{doc\rightarrow bac} + BGEdet \cdot det^{tr} \cdot \tau_{det\rightarrow bac}$
$-bac^{tr} \cdot (\tau_{bac\rightarrow doc} + \tau_{bac\rightarrow det} + \tau_{bac\rightarrow bur} + \tau_{bac\rightarrow mic})$
$-bac^{tr} \cdot (\tau_{bac\rightarrow nem} + \tau_{bac\rightarrow mei} + \tau_{bac\rightarrow mac})$
$\frac{d\ mic^{tr}}{d\ t} = mpb^{tr} \cdot \tau_{mpb\rightarrow mic} + bac^{tr} \cdot \tau_{bac\rightarrow mic}$

$$
\begin{aligned}
&+det^{tr} \cdot \tau_{det \to mic} + doc^{tr} \cdot \tau_{doc \to mic} \\
&-\frac{\sum_i stock_i^{tr} \cdot \tau_{i \to mic}}{\sum_i flow_{i,mic}} \cdot (\tau_{mic \to dic} + \tau_{mic \to det}) \\
&-mic^{tr} \cdot (\tau_{mic \to nem} + \tau_{mic \to mei} + \tau_{mic \to mac}) \\
\frac{d\ nem^{tr}}{d\ t} &= mpb^{tr} \cdot \tau_{mpb \to nem} + bac^{tr} \cdot \tau_{bac \to nem} \\
&+mic^{tr} \cdot \tau_{mic \to nem} + det^{tr} \cdot \tau_{det \to nem} \\
&-\frac{\sum_i stock_i^{tr} \cdot \tau_{i \to nem}}{\sum_i flow_{i,nem}} \cdot (\tau_{nem \to dic} + \tau_{nem \to det}) - nem^{tr} \cdot \tau_{nem \to mac} \\
\frac{d\ mei^{tr}}{d\ t} &= mpb^{tr} \cdot \tau_{mpb \to mei} + bac^{tr} \cdot \tau_{bac \to mei} \\
&+mic^{tr} \cdot \tau_{mic \to mei} + det^{tr} \cdot \tau_{det \to mei} \\
&-\frac{\sum_i stock_i^{tr} \cdot \tau_{i \to mei}}{\sum_i flow_{i,mei}} \cdot (\tau_{mei \to dic} + \tau_{mei \to det}) - mei^{tr} \cdot \tau_{mei \to mac} \\
\frac{d\ mac^{tr}}{d\ t} &= mpb^{tr} \cdot \tau_{mpb \to mac} + bac^{tr} \cdot \tau_{bac \to mac} \\
&+mic^{tr} \cdot \tau_{mic \to mac} + nem^{tr} \cdot \tau_{nem \to mac} \\
&+mei^{tr} \cdot \tau_{mei \to mac} + det^{tr} \cdot \tau_{det \to mac} \\
&-\frac{\sum_i stock_i^{tr} \cdot \tau_{i \to mac}}{\sum_i flow_{i,mac}} \cdot (\tau_{mac \to dic} + \tau_{mac \to det}) - mac^{tr} \cdot \tau_{mac \to exp} \\
\frac{d\ doc^{tr}}{d\ t} &= \Gamma \cdot FixRate \cdot \frac{mpb \to doc}{dic \to mpb} + \frac{\sum_i stock_i^{tr} \cdot \tau_{i \to bac}}{\sum_i flow_{i,bac}} \cdot \tau_{bac \to doc} \\
&-doc^{tr} \cdot (\tau_{doc \to bac} + \tau_{doc \to mic}) \\
\frac{d\ det^{tr}}{d\ t} &= mpb^{tr} \cdot \tau_{mpb \to det} + bac^{tr} \cdot \tau_{bac \to det} \\
&+ \sum_i (stock_i^{tr} \cdot \tau_{i \to mic}) \cdot \frac{mic \to det}{\sum_i flow_{i \to mic}} \\
&+ \sum_i (stock_i^{tr} \cdot \tau_{i \to nem}) \cdot \frac{nem \to det}{\sum_i flow_{i \to nem}} \\
&+ \sum_i (stock_i^{tr} \cdot \tau_{i \to mei}) \cdot \frac{mei \to det}{\sum_i flow_{i \to mei}} \\
&+ \sum_i (stock_i^{tr} \cdot \tau_{i \to mac}) \cdot \frac{mac \to det}{\sum_i flow_{i \to mac}} \\
&-det^{tr} \cdot (\tau_{det \to bac} + \tau_{det \to mic} + \tau_{det \to nem} + \tau_{det \to mei} + \tau_{det \to mac})
\end{aligned}
$$

Finally, the output of each tracer model was evaluated against the experimental data by means of a weighted cost function

$$J = \sum_{i=1}^{nv} \sum_{j=1}^{no} \left(\frac{Mod_{ij} - Obs_{ij}}{\sigma_i \cdot Obs_{ij}} \right)^2 \tag{3.12}$$

where nv is the number of variables, no is the number of observations, Mod_{ij} is the modeled value of the observed counterpart Obs_{ij} and σ_i is the relative weighting factor. Relative errors could not be assessed from the observations but were assigned based on conversion protocols: 0.15 for microphytobenthos and bacteria, 0.10 for nematodes and 0.05 for macrobenthos. Different weighting scenarios were tested but this did not alter the results significantly. The run with the lowest cost function was accepted as CITS.

3.7 Appendix C: Comparison of the inverse solutions CS, CIS and CITS

The inverse solutions, CS, CIS and CITS, are obtained using different data sets and therefore the solutions differ from each other (Table 3.6). The sum of all flows increases with increasing data resolution from 7670 (CS), 8322 (CIS) to 8398 (CITS). The main differences are found between CS and both CIS and CITS (Fig. 3.4). Differences are found over the whole range of flows, the correlation coefficients for CS versus CIS are 0.82 and 0.79 for CS versus CITS. The correlation coefficient for CIS versus CITS amounts 0.99 (Fig. 3.5). While the flows at the lower and higher end agree reasonably, there are still differences between the CIS and the CITS for intermediate sized flows (Fig. 3.5).

Table 3.6: Flow values (mg C m^{-2} d^{-1}) of the inverse solutions CS, CIS and CITS.

Flow	CS	CIS	CITS
doc → bac	586	253	249
doc → mic	129	601	487
det → bac	695	1391	1370
det → mic	515	210	275
det → nem	1	0	0
det → mei	24	0	0
det → mac	20	0	0
phy → det	500	1077	987
phy → mac	520	139	198
spm → det	500	304	334
dic → mpb	714	714	714
mpb → dic	406	114	114
mpb → doc	300	348	300
mpb → det	0	0	0
mpb → mic	0	0	0
mpb → nem	9	17	18
mpb → mei	0	25	25
mpb → mac	0	210	257
bac → dic	683	1047	1021
bac → doc	416	506	436
bac → det	31	37	135
bac → mic	13	13	13
bac → nem	32	14	14
bac → mei	55	0	0
bac → mac	51	28	0
bac → bur	0	0	0
mic → dic	587	710	678
mic → det	0	38	22
mic → nem	9	0	1
mic → mei	33	2	2
mic → mac	29	75	71
nem → dic	8	3	3
nem → det	36	24	24
nem → nem	2	3	2

nem → mac	5	4	6
mei → dic	63	13	13
mei → det	26	6	6
mei → mac	23	8	8
mac → dic	365	226	283
mac → det	162	116	135
mac → exp	122	122	122

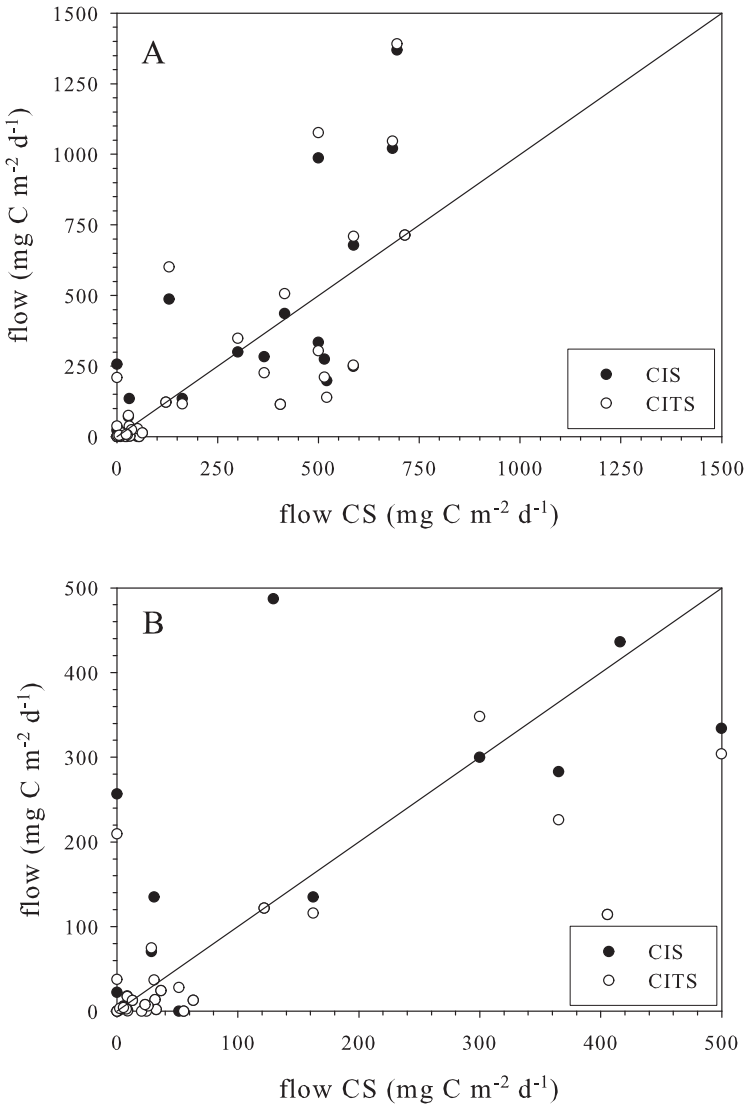

Figure 3.4: Comparison of CIS and CITS with CS on A) a scale from 0 - 1500 mg C m^{-2} d^{-1} and B) a scale from 0 - 500 mg C m^{-2} d^{-1}.

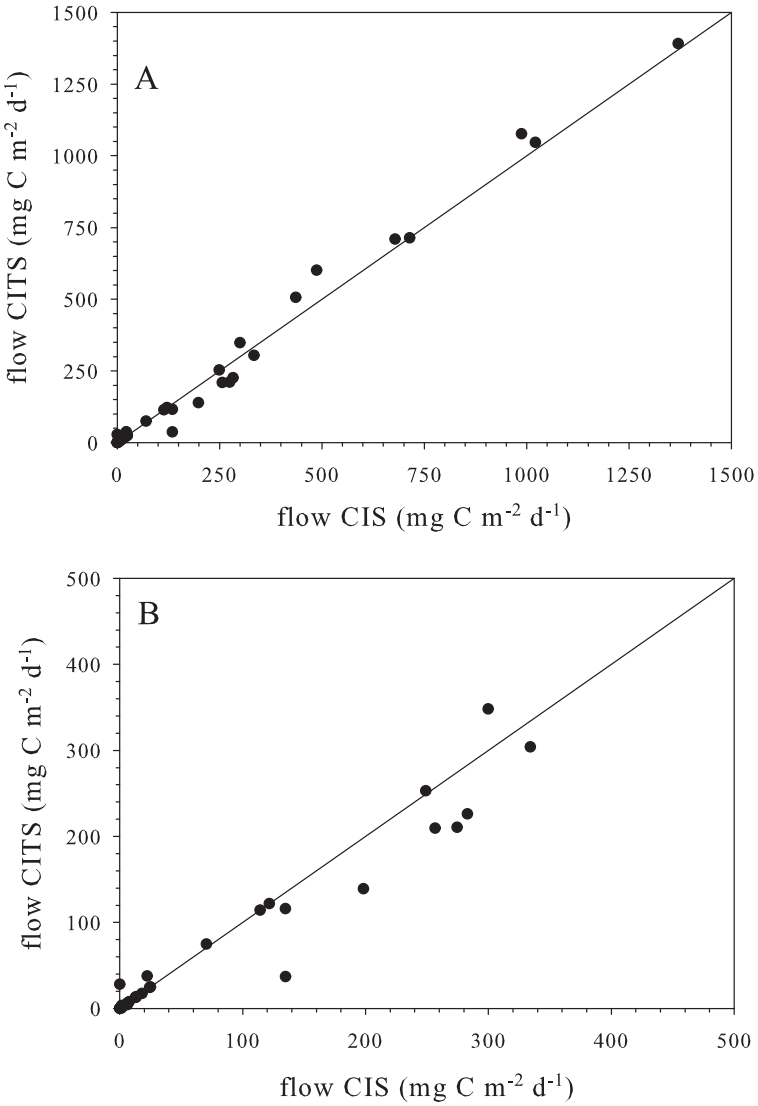

Figure 3.5: Comparison of the CIS with the CITS on A) a scale from 0 - 1500 mg C m^{-2} d^{-1} and B) a scale from 0 - 500 mg C m^{-2} d^{-1}.